Hybrid DSC-T/β-Newmark Method for Dynamic Response Analysis of Isotropic Thin Plates on Elastic Foundations

Mohamed Gibigaye [1], Crespin Prudence Yabi [2], Ezéchiel I. Alloba [2], Ehsan Noroozinejad Farsangi [3,*], and Gerard Degan [2]

[1] University of Abomey-Calavi 01BP 2009, Cotonou, Benin
[2] National University of Sciences, Technologies, Engineering and Mathematics of Abomey, Benin
[3] Faculty of Civil and Surveying Engineering, Graduate University of Advanced Technology, Kerman, Iran
[*] Corresponding author. E-mail: noroozinejad@kgut.ac.ir

Received: Mar. 24, 2020, Accepted: Apr. 24, 2020

The static/dynamic analysis of the thin plate is of great importance in engineering problems. Based on the complexity of the problem, only for some important cases of boundary conditions, analytical solutions were derived. While in general case, numerical approaches should be implemented to solve the problem. The discrete singular convolution (DSC) technique is one of the most accurate methods. Until now, this method is difficult to be used for the determination of the static and dynamic responses for plates with semi-rigid boundary conditions. Based on the fact that DSC method using the *Taylor* approach (DSC-T) is recently used for the analysis of the free vibration of free and semi-rigid edges rectangular plate, this study aims to extend the application of the DSC-T methods to the static and dynamic analysis of the thin rectangular plate restrained with the dowels and resting on elastic foundation. The DSC-T approach is extended to the resolution of the static case of a dowelled plate, and with the combination of the *Newmark* scheme, to the case of the dynamic load. The results showed the applicability of the studied method for the determination of static and dynamic responses of the plates. Besides, it is shown that there is a linear relationship between the value of the depth and the decrement of the modified Vlasov soil. The value of the logarithmic decrement of the soil is highly influenced by the thickness of the plate namely for membranes and very thin plates. The DSC-T method could be recommended for the engineering design of a variety of civil structures.

Keywords: DSC; Newmark scheme; Rigid pavement; Boundary conditions; Elastic foundation; Thin isotropic plate; Taylor series expansion

http://dx.doi.org/10.6180/jase.202009_23(3).0008

1. Introduction

Plates and shells elements have wide applications in practical engineering problems such as aeronautics, biomechanics, petrochemicals, marine industry, mechanics, and civil engineering [1]. During various events such as earthquakes, nuclear explosions, and traffic loadings, these structures may be subjected to transient loads and/or large amplitudes of motion. The dynamic behavior of such thin-walled elements is of great importance in many of the engineering applications, especially for the case of resting on an elastic foundation [2–5]. Due to limitations for the analytical solution, numerical approaches are the most widely used methods for handling these elements [2, 6–10]. In the literature, many methods have been employed to resolve the issue pertaining to governing equations of plates resting on an elastic foundation that are subjected to dynamic load. However, these methods were selected based on the form of the governing equation and mainly on the form of the boundary conditions (BCs).

The discrete singular convolution (DSC) method is a rather interesting method to solve plate problems on the soil [2]. It is one of the most accurate and widely used methods to determine the frequencies and even deflections

of a plate [6, 8, 11].

Due to the high accuracy of the DSC method, many researchers have worked towards extending its application [6, 12–14]. However, implementing boundary conditions using strong-form methods, such as the DSC method, is not an easy task though important [2]. The major problem associated with the DSC method is the presence of fictitious points that increase the number of unknown parameters. The well-known method to take into account the boundary conditions is the symmetric extension, which is mainly used to apply the simply supported boundary conditions [8, 12, 15]. However, for the cases of semi-rigid, free or general boundary conditions they have deficiencies and may encounter problems [2, 6, 13, 16].

To resolve this issue, Wang et al. have implemented Taylor series expansion for thin isotropic and anisotropic plates where the boundary conditions are free edges [11, 13, 16]. However, due to neglection of the DOF of the mixed derivatives, some accuracy and instability issues have happened. Wang and Yuan [6] have proposed conditions for each corner of the investigated plate to avoid free corner conditions. The final outcome from their study was the accuracy and applicability of the Taylor series expansion for the cases of arbitrary boundary conditions. This approach has been used by Gibigaye et al. [2] for the case of a rectangular plate resting on a modified Vlasov soil type. They showed that the DSC method, along with Taylor's approach (DSC-T), is accurate, and is recommended for the dynamic analysis of such plates.

To analyze the dynamic deflection of plates, the DSC method is generally coupled with another method such as differential quadrature (DQ) and harmonically differential quadrature (HDQ) [1]. For time integration, the Runge Kutta and Newmark Scheme are often used along with strong-form methods such as DQM [17–21] and DSC [22]. To model, the dynamic behavior of thin plates based on a modified elastic Vlasov soil type, different time-step integration methods [23] such as Runge-Kutta (RK) [24, 25] or Newmark (NM) [26] are developed. These two methods are often implemented to calculate linear and non-linear transient responses in mechanical systems. However, they are expensive in terms of calculation time due to the inherent disadvantages of each method. Among the family of RK methods, the explicit order-4 scheme (RK4) is the most widely used and is initially used to solve ordinary order-one differential systems. As this one expresses the current state of the system based on its previous state, it is easy to implement. For example, Yang et al. [22] used RK4 to compare the DSC algorithm and the Pseudo Spectral Fourier (FPS) method in solving partial differential equations. However, the time step must be small enough to satisfy the stability condition. Moreover, the size of the system of equations of the dynamic problem is doubled because the system is decomposed into two systems of differential equations of the first order.

The Newmark Method (NM) is a practical method for extremely complex problems. Its results can be sufficiently accurate, even with a time step greater than that of the explicit diagrams for the linear case [27]. However, the need to invert the matrices at each time step penalizes the computation time. Furthermore, non-linearities are often present in the dynamics of mechanical systems, leading to changes in the stability of NM schemes, i.e. unconditional convergence cannot be imposed.

As the governing equation to be solved is linear, the NM proves to be the most appropriate method in this regard, especially as it allows the numerical resolution of second-order differential equations. It is suitable for linear differential systems with a mass matrix and applied force that can depend on both position and time.

This study aims to investigate the effects of the stiffness of the surrounding soil, the thickness of the plate and the depth of the subsoil on the dynamic response of a rectangular thin plate on an elastic foundation. The foundation is a modified Vlasov soil type. To this aim, the application of Taylor series expansion approach has been extended for static/dynamic analyses of the case of dowelled rectangular plates. It was assumed that all edges were elastically restrained using a coupled DSC-T/β-Newmark method. The results of the study are of great importance in rigid pavement modeling, analysis, and design.

2. Modeling of the Soil-Plate System

Figure 1 shows a rectangular thin plate which is isotropic in nature with dimensions of a, b and h, resting on a modified Vlasov soil foundation is depicted in Figure 1. Equation 1 formulates the transverse deflection of the Kirchhoff plate considering the reduced damping of the system and mass of soil [2].

$$\begin{array}{l} D\nabla^4 \mathrm{w}(x,y,t) + k_o \mathrm{w}(x,y,t) - c_o \nabla^2 \mathrm{w}(x,y,t) \\ +c\frac{\partial w(x,y,t)}{\partial t} + (\rho h + m_o)\frac{\partial^2 \mathrm{w}(x,y,t)}{\partial t^2} = P(x,y,t) \end{array} \quad (1)$$

In Equation 1, $\mathrm{w}(x,y,t) = \overline{\mathrm{w}}(x,y,0,t)$. The deflection of the Kirchhoff plate represents the deflection of the coupled plate-soil system; where $\overline{\mathrm{W}}(x,y,z,t)$ indicates the deflection inside the soil layer, which can be defined as $\overline{\mathrm{w}}(x,y,z,t) = \overline{\mathrm{w}}(x,y,0,t)\phi(z)$, and $\phi(z) = \sinh\left[\gamma\left(1-\frac{z}{H_s}\right)\right] / \sinh\gamma$, and is a vertical decay function of soil that must verify whether $\phi(0) = 1$ and $\phi(H_S) = 0$.

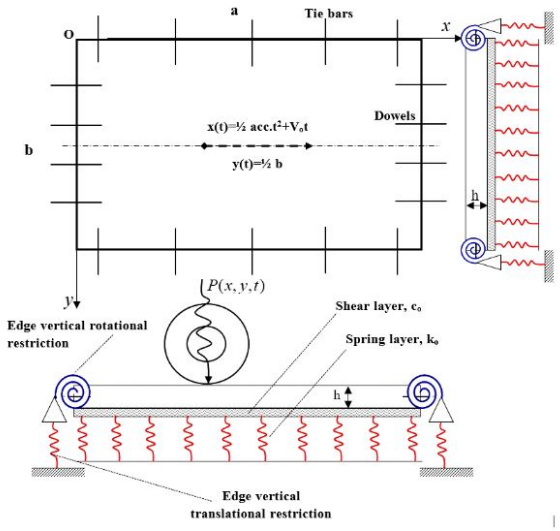

Fig. 1. Modelling of a dowelled plate resting on an elastic foundation.

$P(x,y,t) = P_o\left[1+\frac{1}{2}\cos(\omega t)\right]\delta[x-x(t)]\delta[y-y(t)]$ is the load transmitted to the rectangular plate. Here, $x(t) = v_o t + \frac{1}{2}acc\left(t^2\right)$ and $y(t) = 1/2b$ denote the geometrical position of the load at time t. The magnitude of the moving load is presented by P_0. acc and ω representing the acceleration and angular frequency of the moving load, respectively. δ is the Dirac function. The dimensions of the plate are assumed as a and b, and the flexural stiffness of the element is given by D.

$D = Eh^3/\left(12\left(1-v^2\right)\right)$ is the flexural rigidity of the plate. E, v and h represent the Young's Modulus, the Poisson's ratio and thickness of the plate, respectively. k_0, c_0, and m_0 are integral characteristics of compression, shearing and linear reduced mass of the foundation soil, which is assumed to be homogeneous and mono-layered. They are expressed as follows [2–4]:

$$k_o = \frac{E_o}{1-v_0^2}\int_0^{H_s}[\phi'(z)]^2\,dz = \frac{E_o}{2H_s(1-v_o^2)}\frac{\gamma(\gamma+\sinh\gamma\cosh\gamma)}{(\sinh\gamma)^2} \quad (2)$$

$$c_o = \frac{E_o}{4(1+v_o)}\int_0^{H_s}[\phi(z)]^2 dz = \frac{E_o H_s}{8(1+v_o)}\frac{(\sinh\gamma\cosh\gamma-\gamma)}{\gamma(\sinh\gamma)^2} \quad (3)$$

$$m_o = m\int_0^{H_g}[\phi(z)]^2 dz = \frac{mH_S(\sinh\gamma\cosh\gamma-\gamma)}{2\gamma(\sinh\gamma)^2} \quad (4)$$

In equations 3 and 4, the effective depth of the foundation that is activated dynamically is shown by H_S , the subgrade density is shown by m, and γ is a constant representing the logarithmic decrement of the soil and aids in determining the rate of decrease of the deflections based on the depth of the soil. E_0 represents the Young's Modulus, and v_0 represents the Poisson's ratio.

The BCs in Figure 1 are formulated as follows:

- An array of four generalized equations (5a-5d) were used to model the elastic vertical translation restriction:

$$V_{x=0} = -D\left[\frac{\partial^3 w(0,y,t)}{\partial x^3} + (2-v)\frac{\partial^3 w(0,y,t)}{\partial x\partial y^2}\right] = \left(kS_{soll} + ks_{x1}\right)w(0,y,t) \quad (5a)$$

$$V_{x=a} = D\left[\frac{\partial^3 w(a,y,t)}{\partial x^3} + (2-v)\frac{\partial^3 w(a,y,t)}{\partial x\partial y^2}\right] = \left(ks_{soll} + ks_{x2}\right)w(a,y,t) \quad (5b)$$

$$V_{y=0} = -D\left[\frac{\partial^3 w(x,0,t)}{\partial y^3} + (2-v)\frac{\partial^3 w(x,0,t)}{\partial y\partial x^2}\right] = \left(kS_{soll} + ks_{y1}\right)w(x,0,t) \quad (5c)$$

$$V_{y=b} = D\left[\frac{\partial^3 w(x,b,t)}{\partial y^3} + (2-v)\frac{\partial^3 w(x,b,t)}{\partial y\partial x^2}\right] = \left(ks_{soll} + ks_{y2}\right)w(x,b,t) \quad (5d)$$

In the above equations, $ks_{x1}, ks_{x2}, ks_{y1}, ks_{y2}$ represent the elastic vertical translation stiffness, whereas V_x, V_y representing the vertical shear forces of the plate, and $ks_{soil} = \sqrt{k_0 c_0}$ is the elastic vertical translational stiffness caused by the surrounding soil [28].

- Equations (6a-6d) were used to model the elastic rotation restriction:

$$M_{x=0} = -D\left[\frac{\partial^2 w(0,y,t)}{\partial x^2} + v\frac{\partial^2 w(0,y,t)}{\partial y^2}\right] = \left(kr_{soll} + kr_{x1}\right)\frac{\partial w(0,y,t)}{\partial x} \quad (6a)$$

$$M_{x=a} = D\left[\frac{\partial^2 w(a,y,t)}{\partial x^2} + v\frac{\partial^2 w(a,y,t)}{\partial y^2}\right] = \left(kr_{soll} + kr_{x2}\right)\frac{\partial w(a,y,t)}{\partial x} \quad (6b)$$

$$M_{y=0} = -D\left[\frac{\partial^2 w(x,0,t)}{\partial y^2} + v\frac{\partial^2 w(x,0,t)}{\partial x^2}\right] = \left(kr_{sol} + kr_{y1}\right)\frac{\partial w(x,0,t)}{\partial y} \quad (6c)$$

$$M_{y=b} = D\left[\frac{\partial^2 w(x,b,t)}{\partial y^2} + v\frac{\partial^2 w(x,b,t)}{\partial x^2}\right] = \left(kr_{soll} + kr_{y2}\right)\frac{\partial w(x,b,t)}{\partial y} \quad (6d)$$

$$M_{xy} = -D(1-v)\frac{\partial^2 w(x,y,t)}{\partial x\partial y} = \left(kxy_{soll} + k_{xy}\right)w(x,y,t) \quad (6e)$$

In the above equations, $k_{x1}, k_{x2}, k_{y1}, k_{y2}$ represent the elastic rotational stiffness, whereas M_X, M_Y representing the bending moments of the finite plate, and $kr_{sal} = 1/2\left(c_o\sqrt{k_0/c_0}\right)$ is the elastic rotational stiffness caused by the surrounding soil [**?**].

- The characterization of the elastic torsion at the corners of the plate has been done by Equation 6e.

In the above equation, $(x;y)$ are like $\{(x=0;y=0);(x=0,y=b);(x=a,y=0);(x=a;y=b)\}$; $kxy_{soil} = 3c_0/8$ represents the elastic torsional stiffness at each corner of the plate caused by the surrounding soil

[?], and k_{xy} represents the elastic torsional stiffness at each corner of the plate. The initial conditions (t = 0s) have been characterized as follows:

$$\frac{\partial w(x,y,0)}{\partial t} = w(x,y,0) = 0 \tag{7}$$

For generalization and simplicity, the following dimensionless parameters are introduced:

$X = \frac{x}{a}, Y = \frac{y}{b}, W = \frac{w}{h}, \beta = \frac{a}{b}; C = \frac{ca^4}{D_{11}}; \delta(x - x_0) = \frac{\delta(X - X_0)}{a}$ and $\delta(y - y_0) = \frac{\delta(Y - Y_0)}{b}$

Equation 1 then takes the following form:

$$\begin{aligned} &\frac{\partial^4 W}{\partial X^4} + 2\beta^2 \frac{(D_{12}+2D_{66})}{D_{11}} \frac{\partial^4 W}{\partial X^2 \partial Y^2} + \beta^4 \frac{D_{22}}{D_{11}} \frac{\partial^4 W}{\partial Y^4} + \frac{k_0 a^4}{D_{11}} W \\ &\quad - \frac{C_0 a^2}{D_{11}} \left(\frac{\partial^2 W}{\partial X^2} + \beta^2 \frac{\partial^2 W}{\partial Y^2} \right) + \\ &\quad C \frac{\partial W}{\partial t} + \frac{(\rho h + m_0) a^4}{D_{11}} \frac{\partial^2 W}{\partial t^2} \\ &= \frac{p_o \left[1 + \frac{1}{2}\cos(\omega . t)\right] a^2 \beta}{Dh} \delta(X - X_0)\, \delta(Y - Y_0) \end{aligned} \tag{8}$$

The dynamic analysis of the plate, as described in Figure 1, can be conducted by solving Equation 8 using the boundary conditions indicated by equations 5 and 6 and the initial conditions presented in Equation 7. In the present study, we combined the DSC method with the Taylor series expansion to discretize in spatial dimension and the Newmark scheme to iterate according to the time steps.

3. Solution procedure by coupled DSC and Taylor series expansion

3.1. Static problem for DSC with Taylor Series Expansion (DSC-T)

Let us take the static case of the problem posed in Figure 1. The governing equation of this system has been presented as follows:

$$\begin{aligned} &D_{11} \frac{\partial^4 w}{\partial x^4} + 2(D_{12} + 2D_{22}) \frac{\partial^4 w}{\partial x^2 \partial y^2} + D_{22} \frac{\partial^4 w}{\partial y^4} \\ &\quad + k_0 w - C_0 \left(\frac{\partial^2 w}{\partial x^2} + \frac{\partial^2 w}{\partial y^2} \right) = q(x,y) \end{aligned} \tag{9}$$

In the above equation, $q(x,y)$ represents the concentrated load, which is applied at the middle of the plate at the point (x_0, y_0) , which can be represented as follows:

$q(x,y) = P\delta(x - x_0)\, \delta(y - y_0)$

The dimensionless of Equation 9 can be represented as follows:

$$\begin{aligned} &D_{11} \frac{\partial^4 w}{\partial x^4} + 2(D_{12} + 2D_{22}) \frac{\partial^4 w}{\partial x^2 \partial y^2} + D_{22} \frac{\partial^4 w}{\partial y^4} \\ &\quad + k_0 w - C_0 \left(\frac{\partial^2 w}{\partial x^2} + \frac{\partial^2 w}{\partial y^2} \right) = q(x,y) \end{aligned} \tag{10}$$

As the properties of the Dirac delta function are in the integral form [19], the DSC method cannot take into account the concerning problem. To overcome this difficulty, previous authors [21, 29] have proposed an approximation for the Dirac delta function with two spatial variables, as shown in Figure 2. The Dirac delta approximation can be

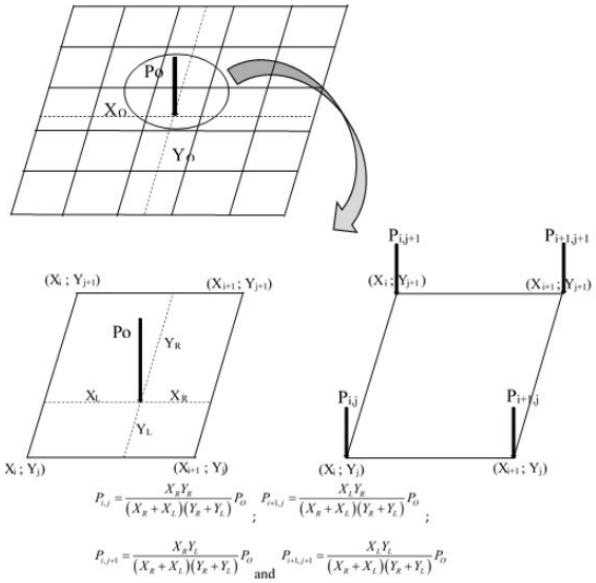

Fig. 2. Equivalent forces at the corners representing a concentrated load [19].

represented as follows:

$$\delta(X - X_0)\, \delta(Y - Y_0) = \frac{1}{(X_R + X_L)(Y_R + Y_L)(\Delta X \Delta Y)} \begin{cases} X_R Y_R; & (X_t, Y_j) \\ X_L Y_R; & (X_{t+1}, Y_j) \\ X_R Y_L; & (X_i, Y_{j+1}) \\ X_L Y_L; & (X_{i+1}, Y_{j+1}) \\ 0 & \text{otherwise} \end{cases} \tag{11}$$

In the above equation,ΔX and ΔY represent the average spacing of grid points in x and y directions, respectively. This approach was used by Wang [29], and it produces accurate results when $\Delta X \to 0$ and $\Delta Y \to 0$, i.e. when the grid number increases.

3.2. Discretization of the thin rectangular plate by the DSC-T

To cope with the BCs and the governing equations, the DSC algorithm has been adopted. Equation 12 shows approximated n^{th} order derivative of a function W(x) using the DSC algorithm, via a discretized convolution [13, 29–31]:

$$W^{(n)}(x) \approx \sum_{k=-M}^{M} \delta_{\sigma,\Delta}^{(n)}(x - x_k)\, W(x_k) \quad (n = 1, 2, \ldots) \tag{12}$$

In the above equation, the computational bandwidth is 2M+1, and x^k $(k = -M, ..., -1, 0, 1, ...M)$ represent uniformly distributed grid points. The superscript (n) denotes the n^{th} order derivative with respect to x . $\delta_{\sigma,\Delta}^{(n)}(x - x_k)$ is

a collection symbol for the DSC kernels, and its nth order derivative is represented by Equation 13:

$$\delta^{(n)}_{\sigma,\Delta}(x-x_k)=\left(\frac{d}{dx}\right)^n\delta_{\sigma,\Delta}(x-x_k),\quad (n=1,2,\dots) \tag{13}$$

Due to the efficiency and accuracy of the regularised Shannon's delta sequence kernel (DSC-RSK), it is used for the differential terms of the equation as shown in Equation 14.

$$\delta_{\sigma,\Delta}(x-x_k)=\frac{\sin[\pi/\Delta(x-x_k)]}{\pi/\Delta(x-x_k)}\exp\left[-\frac{(x-x_k)^2}{2\sigma^2}\right] \tag{14}$$

In the above equation, σ is a controllable parameter, and $\Delta = x_k - x_{k-1}$ represents the spacing between two grid points. The parameter σ aids in determining the width of the Gaussian envelope and often varies in association with the grid spacing $\sigma = r \times \Delta$ where r is a parameter chosen to obtain a stable solution to the problem in the computation stage.

Equation 15 shows a uniform grid considered in this study:

$$\begin{gathered}0=X_0<X_1<\cdots<X_N=1 \text{ and },\\ 0=Y_0<Y_1<\cdots<Y_N=1\end{gathered} \tag{15}$$

To eliminate the fictitious points, and also handling general BCs, a numerical algorithm should be provided. In this work, the Taylor series expansion method [13] is used to eliminate the M fictitious DOFs outside the physical domain of the plate. The Taylor series expansions for w(x) and w(-x) at x_0 was developed in earlier studies [2, 6]. They have been listed as follows:

$$\begin{gathered}\mathrm{w}(x)=\mathrm{w}(x_o)+\mathrm{w}^{(1)}(x_o)(x-x_o)\\ +\tfrac{1}{2!}\mathrm{w}^{(2)}(x_o)(x-x_o)^2\\ +\tfrac{1}{3!}\mathrm{w}^{(3)}(x_o)(x-x_o)^3+\tfrac{1}{4!}\mathrm{w}^{(4)}(x_o)(x-x_o)^4+\\ +\tfrac{1}{5!}\mathrm{w}^{(5)}(x_o)(x-x_o)^5+\dots\end{gathered} \tag{16}$$

$$\begin{gathered}\mathrm{w}[-(x)]=\mathrm{w}(x_o)-\mathrm{w}^{(1)}(x_o)(x-x_o)\\ +\tfrac{1}{2!}\mathrm{w}^{(2)}(x_o)(x-x_o)^2\\ -\tfrac{1}{3!}\mathrm{w}^{(3)}(x_o)(x-x_o)^3+\tfrac{1}{4!}\mathrm{w}^{(4)}(x_o)(x-x_o)^4+\\ -\tfrac{1}{5!}\mathrm{w}^{(5)}(x_o)(x-x_o)^5+\dots\end{gathered} \tag{17}$$

According to a few authors [6, 11, 29, 32], the sum of equations 16 and 17 is more accurate than their difference for applying the boundary conditions by DSC. Thus, we summed these equations and obtained, considering the second and fourth-order derivative, respectively, equations 18 and 19.

$$\begin{gathered}\mathrm{w}[-(x)]=-\mathrm{w}(x)+2\mathrm{w}(x_o)\\ +\mathrm{w}^{(2)}(x_o)(x-x_o)^2\qquad x>xo\end{gathered} \tag{18}$$

$$\begin{gathered}\mathrm{w}[-(x)]=-\mathrm{w}(x)+2\mathrm{w}(x_o)+\mathrm{w}^{(2)}(x_o)(x-x_o)^2\\ +\tfrac{1}{12}\mathrm{w}^{(4)}(x_o)(x-x_o)^4\quad x>xo\end{gathered} \tag{19}$$

For the boundary value problems with second-order differential equations, if only one additional DOF is needed, then Equation 18 is used. For the case of two additional degrees of freedom, Equation 19 can be used.

Instead of just using Equation 19, both equations 18 and 19 can be used for computational efficiency by eliminating the DOFs on the M fictitious points outside the domain of the plate. In the current study, this approach has been used for general BCs.

To discretize Equation 10, we used the method presented by Wang and Yuan [6] and Gibigaye et al. [2]. For the purpose of simplification, we only presented the derivation in direction x. We assumed that the computational bandwidth 2M + 1 is less than or equal to N. Therefore, the first M fictitious points only affect the first M equations, and the last M fictitious points affect the last M equations. After eliminating all DOFs at the fictitious points, the nth order derivatives with respect to x for the DSC and their "weighting coefficients" can be presented as Equation 20:

$$\begin{gathered}\mathrm{w}^{(n)}(x_i)=\sum_{k=1}^{N}F^{(n)}_{i,k}\mathrm{w}(x_k)+F^{(n)}_{i,N+1}\mathrm{w}^{(2)}(x_1)+F^{(n)}_{i,N+2}\\ \mathrm{w}^{(4)}(x_1)+F^{(n)}_{i,N+3}\mathrm{w}^{(2)}(x_N)+F^{(n)}_{i,N+4}\mathrm{w}^{(4)}(x_N)\\ \mathrm{w}^{(n)}(x_i)=\sum_{k=1}^{N+4}\tilde{F}^{(n)}_{i,k}\tilde{\mathrm{w}}(x_k)\end{gathered} \tag{20}$$

The parameters in the above equation are described as follows:

$$F^{(n)}_{i,k}=\begin{cases}C^{(n)}_{i,k-i}+\sum_{k=2}^{2+M-i}2C^{(n)}_{i,2-k-i} & \text{If, k = 1}\\ C^{(n)}_{i,k}-C^{(n)}_{i,2-k-i}-C^{(n)}_{i,2N-k-i} & \text{If,k = 2,3,...N - 1}\\ C^{(n)}_{i,k-i}+\sum_{k=2N-M-i}^{N-1}2C^{(n)}_{i,2N-k-i} & \text{if, k = N}\end{cases}$$

$$\begin{aligned}&F^{(n)}_{i,N+1}=\sum_{k=2}^{2+M-i}\tfrac{1}{12}C^{(n)}_{i,2-k-i}(x_k-x_1)^2;\\ &F^{(n)}_{i,N+2}=\sum_{k=2}^{2+M-i}\tfrac{1}{12}C^{(n)}_{i,2-k-i}(x_k-x_1)^4\\ &F^{(n)}_{i,N+3}=\sum_{k=2N-M-i}^{N-1}\tfrac{1}{12}C^{(n)}_{i,2N-k-i}(x_N-x_k)^2;\\ &F^{(n)}_{i,N+4}=\sum_{k=2N-M-i}^{N-1}\tfrac{1}{12}C^{(n)}_{i,2N-k-i}(x_N-x_k)^4\end{aligned}$$

In the above equations, $F^{(n)}_{i,j}$ represent the weighting coefficients of the nth order derivative with respect to x at point $x_i = (i-1)\Delta x$. N represents the number of grid points $\Delta x = 1/(N-1)$, and $\widetilde{W}$ is apparent. These variables are considered to be dimensionless. In case the weighting coefficients of one dimension are known in the above formulations, the static analysis of a rectangular thin plate using the DSC-T approach cab be conducted directly.

In terms of DSC, Equation 10 at all grid points can be expressed in the form of Equation 21:

$$\begin{array}{l}\sum_{k=1}^{Nx+4} D_{i,k}^{x}\tilde{W}_{kj}+2\beta^2\sum_{k=1}^{Nx+4}\sum_{l=1}^{Ny+4} B_{i,k}^{x}B_{j,l}^{y}\tilde{W}_{kl}\\ +\beta^4\sum_{l=1}^{Ny+4} D_{j,k}^{y}\tilde{W}_{il}+K_r\tilde{W}_{ij}+\\ C_r\left(\sum_{l=1}^{Nx+4} B_{i,k}^{x}\tilde{V}_{kj}+\beta^2\sum_{l=1}^{Ny+4} B_{j,l}^{y}\tilde{W}_{il}\right)\end{array} = \frac{Pa^2\beta}{Dh}\frac{1}{(X_R+X_L)(Y_R+Y_L)(\Delta X\Delta Y)}\begin{cases} X_RY_R; & \left(X_i,Y_j\right)\\ X_LY_R; & \left(X_{i+1},Y_j\right)\\ X_RY_L; & \left(X_i,Y_{j+1}\right)\\ X_LY_L; & \left(X_{i+1},Y_{j+1}\right)\\ 0 & \text{otherwise}\end{cases}$$
$$i=1,2,\ldots,Nx; j=1,2,\ldots,Ny \tag{21}$$

In the above equation,$D_{i,k}^{x}$, $D_{j,l}^{y}$, $B_{i,k}^{x}$ and $B_{j,l}^{y}$ are the weighting coefficients of the 4th and 2nd -order derivatives with respect to x or y; that are calculated using Equation 20. N_x and N_y are the number of grid points in x and y directions. We chose N_x=N_y=N. The DOFs $\tilde{W}_{kl}$ contain the following: i) the deflection W at all grid points, ii) its second and fourth-order derivatives with respect to x or y at all boundary points and iii) the mixed order derivatives at the four corner points. Following this, we derived $(N+4)x(N+4)$ DOFs in total.

The governing equation is used at all NxN grid points. To ease the programming effort and maintain accuracy, the $8N+4$ DOFs, involving the 2nh and 4th-order derivatives, were considered as fictitious points outside the plate domain.

It should be noted that for convenience of programming, additional grid points were introduced in Equation 12 which are not fictitious points. The remaining DOFs at the corners are demonstrated to be null [6] for governing equations of the isotropic and anisotropic thin plates.

To eliminate the DOFs at the fictitious points outside the plate, the weighting coefficients of the 3rd - and 4th -order derivatives are calculated using Equation 19 again. Instead of using Equation 19, Equation 19 is used to formulate the weighting coefficients of the 1st - and 2nd -order derivatives, as follows:

$$\begin{array}{c}\mathrm{w}^{(n)}(x_i)\approx\sum_{k=1}^{N}F_{i,k}^{(n)}\mathrm{w}(x_k)+F_{i,N+1}^{(n)}\mathrm{w}^{(2)}(x_1)\\ +(0)\mathrm{w}^{(4)}(x_1)+F_{i,N+3}^{(n)}\mathrm{w}^{(2)}(x_N)+(0)\mathrm{w}^{(4)}(x_N)\\ =\sum_{k=1}^{N+4}\tilde{F}_{i,k}^{(n)}\tilde{\mathrm{W}}(x_k)\\ i=1,2,\ldots,N;\text{ and } n=1,2\end{array} \tag{22}$$

In the above equation, the variables $F_{i,j}^{(n)}$, N and Δx are the same as in Equation 20.

For convenience, the weighting coefficients of the 1st - to 4th -order derivatives are denoted by $A_{i,j}, B_{i,j}, C_{i,j}$ and $D_{i,j}$. Thus, the form of the discrete governing equation remains as indicated in Equation 21. Therefore, the total number of DOFs in Equation 21 was reduced to N^2+8N+4 .

3.3. Static response of thin rectangular plate by DSC-T

To resolve the static case of the problem, posed in section 2, BC equations in terms of the DSC had to be added to Equation 21. Following this, all necessary equations were obtained. The displacement vector can be expressed in the form of a partitioned matrix as shown in Equation 23:

$$\begin{bmatrix}[K_{\alpha\alpha}] & \begin{bmatrix}K_{\alpha\beta}\end{bmatrix}\\ \begin{bmatrix}K_{\beta\alpha}\end{bmatrix} & \begin{bmatrix}K_{\beta\beta}\end{bmatrix}\end{bmatrix}\begin{Bmatrix}\{W_\alpha\}\\ \{W_\beta\}\end{Bmatrix}=\kappa\{P\} \tag{23}$$

In the above equation, $\{P\}$ represents the concentrated load, as defined in [19]. $\{W_\alpha\}$ contains only the displacement DOFs; its dimensions depend on the combinations of boundary conditions and $\kappa=\frac{a^2\beta}{Dh\Delta X\Delta Y}$

After eliminating $\{W_\beta\}$, Equation 22 can be restored to a standard linear system equation as follows:

$$[\bar{K}]\{W_\alpha\}=\kappa\{P\} \tag{24}$$

In the Eq. 24,

$$[\bar{K}]=\left[K_{\alpha\alpha}-K_{\alpha\beta}K_{\beta\beta}^{-1}K_{\beta\alpha}\right] \tag{25}$$

The deflections can be obtained using a standard linear equation system solver.

3.4. Dynamic response of the plate applying the β-Newmark scheme

3.4.1. *Principle of Newmark's method*

Consider the following to be a general form of a dynamic equation:

$$M\ddot{W}+C\dot{W}+KW=P \tag{26}$$

In the above equation, W is the displacement vector, M,C,K and P represent the mass, the damping, the stiffness and the applied load matrices, respectively.

The principle of the Newmark method is to determine, based on limited development, the position (W) and the velocity () at time t_{i+1} using the value of time t_i . This development includes an error term of the third order that is proportional to the derivative of acceleration. Several hypotheses of the NM method allow replacing the third-order derivative with the acceleration recorded during the previous time, introducing two parameters γ and β . It can be represented using the following correction scheme:

$$\begin{array}{c}W_{i+1}=W_i+h_p\dot{W}_i+(h_p)^2\left[\left(\frac{1}{2}-\beta\right)\ddot{W}_i+\beta\ddot{W}_{i+1}\right]\\ \dot{W}_{i+1}=\dot{W}_i+h_p\left[(1-\gamma)\ddot{W}_i+\gamma\ddot{W}_{i+1}\right]\end{array} \tag{27}$$

According to Géradin and Rixen [34], for $\gamma=1/2$ and $\beta=1/4$, the $\beta-$ Newmark method is implicit and unconditionally stable. In that case, the acceleration is supposed to not vary within the range $[t_i,t_{i+1}]$ [33]. Therefore, the method of mean acceleration will be used in this work.

3.4.2. Algorithm

The algorithm for the β-Newmark method for linear systems is presented as follows [34]:

- At t=0 (when the plate doesn't exhibit any deformation or motion), if $\dot{W}_0 = 0$ and $W_0 = 0$, then

$$\ddot{W}_0 = M^{-1}\left(P_0 - C\dot{W}_0 - KW_0\right) \tag{28}$$

The state of the problem at time t_n is supposed to be known: $W_n, W_n, \dot{W}_n$

- Prediction

$$\begin{aligned} W_{n+1} &= W_n + h_p\dot{W}_n + \left(\tfrac{1}{2} - \beta\right)h_p^2\ddot{W}_n \\ \dot{W}_{n+1} &= \dot{W}_n + (1-\gamma)h_p\ddot{W}_n \end{aligned} \tag{29}$$

- Correction

$$\begin{aligned} \ddot{W}_{n+1} &= \left(M + \gamma h_p C + \beta h_p^2 K\right)^{-1}\left(P_{n+1} - C\dot{W}_{n+1} - KW_{n+1}\right) \\ W_{n+1} &= W_{n+1} + \beta h_p^2\ddot{W}_{n+1} \\ \dot{W}_{n+1} &= \dot{W}_{n+1} + \gamma h_p\ddot{W}_{n+1} \end{aligned} \tag{30}$$

In the above equations, γ and β are the two parameters of the β-Newmark method, and h_p is the time step.

4. Results and Discussion

An important stage of such studies is to verify the applicability of proposed formulations. To this aim, two simply supported S-S-S-S, semi-rigid or elastic edges and E-E-E-E boundary conditions have been considered. The corresponding stiffnesses for the restraining springs have been specified in Table 1. Using the proposed procedure, the response of an isotropic plate resting on an elastic foundation was analyzed. A finite rectangular plate of 3.5 m $\times$5 m $\times$ 0.25 m, dowelled along its edges, was considered, as shown in Figure 1. The structural properties of the plate have been listed as follows: density $\rho = 2500\text{kg}\cdot\text{m}^{-3}$, Poisson's ratio $v = 0.25$, and longitudinal elastic modulus $E = 24\times10^9 Pa$. The density of the subgrade has been $m = 1800\text{kg}\cdot\text{m}^{-3}$; its Poisson's ratio has been $v_S = 0.35$ and longitudinal elastic modulus was $E_S = 50.10^6 Pa$ [4, 35]. For the purpose of validation and comparison, the plate with simple boundary conditions was analyzed. From the generalized boundary conditions, we obtained the simple one.

4.1. Validation of the DSC-T method according to deflections

To validate the used method, we compared the deflections at the center of the plate by using the DSC-T to evaluate the static loading of the plate, which was considered as simply supported at its edges, with those obtained from the analytical Navier's method. Based on the previous study [2] that we used to validate the DSC-T method, $N = 19$ and $r = 3$ for the DSC-T method, $N = 19$ and $r = 3$ for Navier's method, $n = m = 79$ mode numbers in each direction. For the DSC-T method, we used the calculation code Mathematica 9.0 in conformity with the algorithm described in Section 3. The maximal deflection obtained at the center of the plate with the DSC-T was $W_{max} = 0.002778m/m$. The maximal deflection obtained analytically using Navier's approach was $W_{max} = 0.002783m/m$. Thus, the relative error was found to be 0.18%. The obtained relative error is acceptable for the engineering design of civil structures. Thus, the DSC-T method is sufficiently accurate to analyse the studied plate.

4.2. Study of the static case

For the modified Vlasov soil, we implemented the iterative algorithm to determine the logarithmic decrement γ , as presented by Turhan and Straughan [2, 4**? ?**]. We gave the calculation code based on Mathematica 9.0 in the supplementary data. The results obtained for different soil depths and displacements, corresponding to each decrement value γ , have been presented in Table 2.

Based on these data and by varying the thickness of the plate, we plotted two curves: the curve of variation of the logarithmic decrement as a function of the depth H_S for different thicknesses of the plate (Figure 3) and the variation of the deflection as a function of the depth of the soil (Figure 4).

4.2.1. Effect of soil depth on γ values at different thicknesses of the plate

Figure 3 shows that the curves are linear, irrespective of the thickness of the plate (0.1 m, 0.2 m, 0.3 m, 0.4 m, 0.5 m and 0.6 m). Thus, the logarithmic decrement is concluded to be proportional to the dynamically activated depth of the soil. The ratio of proportionality decreases as the thickness of the plate increases. It varied from 4.75 for h = 0.1 m to 2.74 for h = 0.6 m. From this, we can deduce that the expression of logarithmic decrement can be reduced to γ=αH_s. Even data from Straughan's (1990) [**?**] work leads to deducing this relationship. However, it should be noted that the author did not derive this linear relationship. The linear relationship between γ and H_s is very useful, as knowing the value of γ corresponding to a single depth H_s for the same plate thickness can aid in defining the coefficient of proportionality γ. Thus, the value of γ can be defined for any other dynamically activated depth (for the same plate thickness) without using an iterative approach.

4.2.2. Effect of soil depth on deflection values at different thicknesses

Figure 4 shows that the curves grow and become constant at given depths for each thickness of the plate. Irrespec-

Table 1. The mechanical properties of tie bars and dowels for various BCs [2]

	S-S-S-S edges	E-E-E-E edges
Elastic vertical restraint,$kx, ky(N/m)$	200 E+18	200 E+6
Elastic rotational restraint,$krx, kry(N.m/rad)$	0	1.0 E+6
Elastic torsional restraint,$kxy(N/m^2)$	0	0

Table 2. Values of the logarithmic decrement of the soil γ , and the displacements of the plate of thickness 0.25m

Depth of soil Hs (m)	Value of γ	Number of iterations	Deflection W(m/m)
0.5	1.3827	3	0.000547
1.0	2.4647	4	0.000694
1.5	3.6004	5	0.000729
2.0	4.7784	5	0.000735
2.5	5.9723	6	0.000735
3.0	7.1659	6	0.000735
3.5	8.3598	6	0.000735
4.0	9.5565	6	0.000735
4.5	10.7508	7	0.000735
5.0	11.9449	7	0.000735
5.5	13.1385	7	0.000735
6.0	14.3353	7	0.000735
6.5	15.5297	7	0.000735
7.0	16.7239	7	0.000735

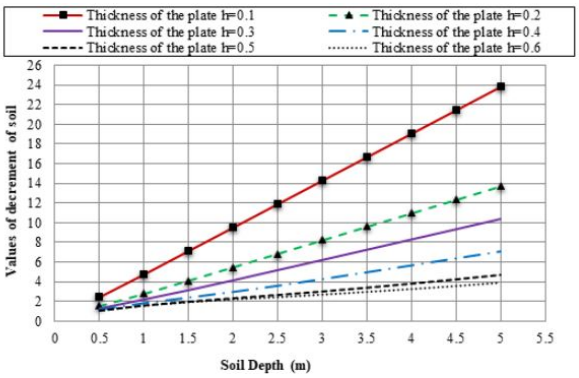

Fig. 3. Variation of logarithmic decrement vs. soil depth at different plate thicknesses.

tive of the thickness of the plate, the deflection converges towards a well-defined value of the depth of the soil. The lower the thickness of the plate, the faster this convergence is reached. Thus, for h = 0.2 m, the deflection converges at a depth of 1.5 m, whereas for h = 0.7 m, convergence is only achieved at a depth of 4 m. From this, we can deduce that beyond a certain depth of soil, deflection stops varying, i.e. a certain soil height is sensitive to the load that is applied on the plate. This depth of soil will be considered in the dynamic case as the dynamically activated depth of soil. It increases as the plate becomes thicker. This implies that soil below this depth has no significant impact on the response of the pavement plate. Thus, soil beyond this depth can be considered as a rigid substratum.

The concept of dynamically activated soil depth could be used to stimulate plate modeling in the case of a dynamic load with the assurance that the impact that the soil can have on the dynamic response of the plate can be controlled. Furthermore, soil can be modeled as a finite medium. In the remaining sections, we will focus on the determined dynamically activated depth of soil.

4.2.3. *Influence of the thickness of the plate on the values of deflections and* γ

To analyse the influence of plate thickness on the logarithmic decrement γ and deflection values, we determined the values of γ as a function of the thickness of the pavement plate at different depths of the soil, as shown in Table 3.

Figure 5 shows that the logarithmic decrement of the soil decreases as the thickness of the plate increases and stabilizes at h = 0.5 m. This implies that for a plate thicker than 0.5 m, the value of soil's logarithmic decrement varies very slightly. Following further verification, it can be concluded that for thicker plates, the value of the logarithmic decre-

Table 3. Value of deflections according to the depth and logarithmic decrement of soil for different thicknesses of the plate

Depth (m)		Thickness of the plate (m)						
		0.1	0.2	0.3	0.4	0.5	0.6	0.7
	Deflection	0.0044	0.000919	0.0003585	0.0001857	0.000112	0.000076	5.559E-05
Hs=0.5m	γ	2.442	1.523	1.298	1.1652	1.091	1.1034	1.1649
	Deflection	0.00464	0.00112	0.0004693	0.000256	0.000161	0.000111	8.381E-05
Hs=1.0m	γ	4.7595	2.7821	2.0025	1.81717	1.62	1.6063	1.6561
	Deflection	0.00465	0.00115	0.0005064	0.000295	0.000214	0.0001365	0.0001036
Hs=1.5m	γ	7.1251	4.117	3.1664	2.3822	2.01	1.9537	1.995
	Deflection	0.00465	0.00115	0.000515	0.000315	0.000225	0.0001544	0.0001184
Hs=2.0m	γ	9.5156	5.4836	4.17022	2.955	2.358	2.25	2.2784
	Deflection	0.00465	0.00115	0.0005165	0.00032	0.0002301	0.000167	0.0001544
Hs=2.5m	γ	11.8922	6.8532	5.203	3.581	2.6967	2.526	2.45484
	Deflection	0.00465	0.00115	0.0005168	0.000327	0.00024	0.000177	0.0001643
Hs=3.0m	γ	14.2731	8.223	6.24044	4.2516	3.0545	2.806	2.71378
	Deflection	0.00465	0.00115	0.0005169	0.0003288	0.000246	0.000184	0.0001715
Hs=3.5m	γ	16.6519	9.596	7.2793	4.9424	3.4384	3.093	2.98503
	Deflection	0.00465	0.00115	0.0005166	0.000329	0.000249	0.000189	0.0001767
Hs=4.0m	γ	19.03	10.966	8.3231	5.6391	3.851	3.4058	3.27063
	Deflection	0.00465	0.00115	0.000516	0.000329	0.0002514	0.000192	0.0001805
Hs=4.5m	γ	21.4094	12.338	9.3632	6.3469	4.284	3.741	3.5681
	Deflection	0.00465	0.00115	0.000516	0.000329	0.0002523	0.0001937	0.0001827
Hs=5.0m	γ	23.788	13.7095	10.4033	7.05047	4.735	4.098	3.89325

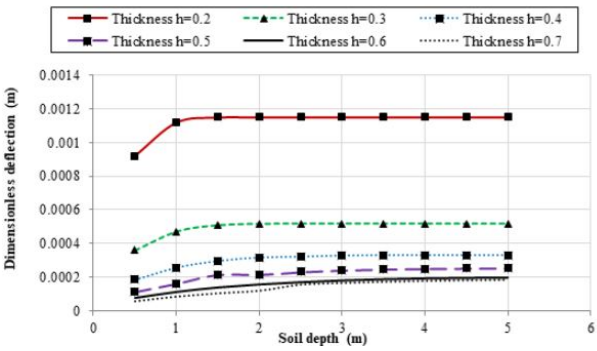

Fig. 4. Variation of the deflection as a function of the depth of the soil at different thicknesses (h) of the plate.

ment varies slightly. From this, we can conclude that the value of the logarithmic decrement of soil is highly influenced by the thickness of the plate, namely, for membranes and very thin plates. For plates of medium thickness and thick plates, the influence of plate thickness on the value of logarithmic decrement is negligible.

Figure 6 shows that the curves are almost mixed up at different depths of soil. The variation in deflection according to thickness does not depend on the depth of the soil. Thus, the depth of soil does not significantly impact the deflection at different values of plate thickness. Furthermore, the deflection of the plate decreases quickly for thicknesses between 0.1m and 0.2 m. Between 0.2 m and 0.4 m, this decline slows down before stabilizing at h = 0.5 m. This implies that deflections decrease when the plate has a medium thickness, and they become constant when the plate is thick.

4.3. Study of the dynamic case

For the dynamic case, we studied the deflection of the plate on Winkler soil, Pasternak soil and modified Vlasov soil. With respect to these different types of soil, we studied the influence of several parameters on the deflection of the plate, namely, the comparison between the static case and the dynamic one, the effect of the inertia of soil, the effect of the damping coefficient and the effect of the stiffnesses of the surrounding soil.

4.3.1. Comparative study between static and the dynamic deflection

Figure 5 demonstrates the variation in deflection along the central axis of the plate ($0 \leq x \leq 5$ m, y = 1.75 m) when a static load is applied at the center of the plate; this

was examined with respect to different types of soil. The curves in the figure show that deflections initially increase; after reaching a peak, they begin to decrease. This can be explained by the fact that deflection is maximum at the point of application of the load; it decreases as it moves away from it. Furthermore, it can be observed that with respect to static loading, deflections are more significant on the Winkler soil with a difference of 18.83% compared to deflections on the Pasternak soil; with respect to deflections on the Vlasov soil, deflections on the Winkler soil generated a difference of 14.72%. This suggests that the plate on Winkler's soil is oversized. This finding is consistent with that of Gibigaye et al.'s [4] who used the modified Bolotin approach to solve a similar problem for a dynamic case. Additionally, we found that deflections on the Pasternak soil are slightly higher than that on the Vlasov soil with a variation of 7.83%. This allows us to conclude that the Vlasov soil can replace the Pasternak soil, which is closer to reality according to several references [36–43].

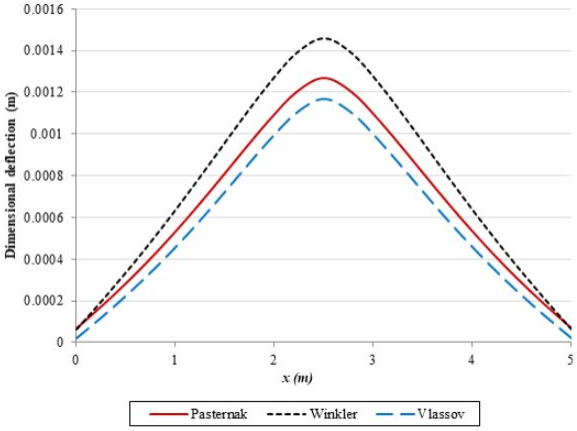

Fig. 5. Variation in deflection along the axis ($0 \leq$ x $\leq$ 5m, y = 1.75 m) for the case of a static load

For the static case, Figure 6, shows that deflections of the plate are higher in the case of Winkler's soil than those on Pasternak and Vlasov soils. It should be noted that deflections on the Vlasov soil type are similar to those on the Pasternak soil, which is considered to be the reference point. We can deduce that compared to the plate on the Pasternak soil, the plate on Winkler's soil is oversized, as can be noticed in the case of static loading. As a rigid pavement can be modeled as presented in Figure 1, in terms of the effective cost of pavement, it would be recommended to avoid using the Winkler soil type in modeling a rigid pavement.

On the other hand, with a modified Vlasov soil type, the value of the dimensionless deflection obtained at the center of the plate $(x = a/2 and y = b/2)$ for the static case is Wmax= 0.00117042, whereas for the dynamic case on the Vlasov soil, Wmax = 0.00200737. Thus, the maximum dynamic dimensionless deflection on the modified Vlasov soil represents 171.50% of the static deflection. This can be explained by the fact that the harmonic load at the center of the plate is 119798.041 N or 49.74% more than the load in the static case where it is only 80000 N. This implies that even without the vibration aspect of the load, i.e. for a uniform load of a magnitude of 80000 N, the dynamic deflection would be higher than the static deflection of 21.76%. From all these observations, we can deduce that the dynamic case has a significant effect on a dynamic system's response. Therefore, it is important to consider the dynamic effect of loading while designing dynamic systems.

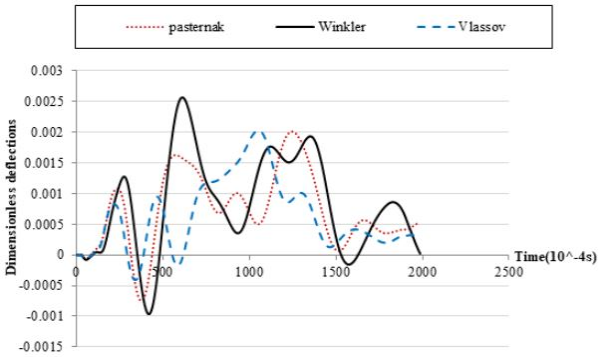

Fig. 6. Deflection at the centre of the plate ($0 \leq$ x $\leq$ 5m, y = 1.75m) for dynamic loading at t = 0.996s

4.3.2. Effect of the inertia of soil on deflections of a plate

Figures 7-9 show variations in plate deflection for different values of Young's modulus of soil at a certain point (x = 0m; y = 1.75m). Analyzing these curves leads to the observation that deflections of a plate on an inertial soil are higher (up to 10%) than those observed on an un-inertial soil, particularly while beginning to apply a load, i.e. around t = 0s. Furthermore, we found that the effect of inertia decreases until the effect reverses, i.e. deflections on the un-inertial soil increase compared to those on the inertial one for values of the modulus of elasticity beginning from Es = 75MPa. This implied that it is important to take into account the inertia of soil up to a certain value of Young's modulus of soil. Therefore, the influence of soil inertia depends on the modulus of elasticity of soil. Following studying the effect of soil inertia at one point of the plate, it would be recommended to study the effect on other points to formulate a general conclusion.

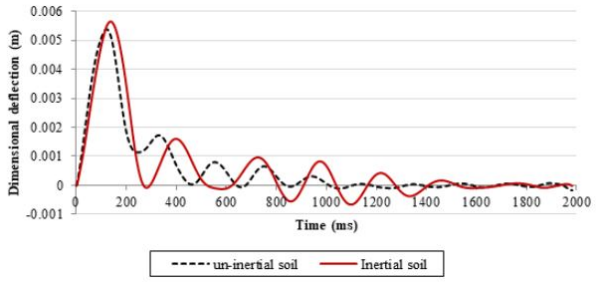

Fig. 7. Effect of inertia on a modified Vlasov soil type for Es = 25MPa

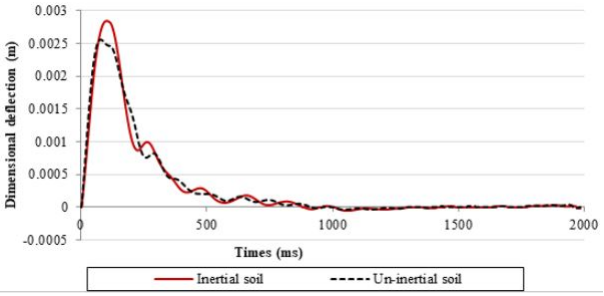

Fig. 8. Effect of inertia on a modified Vlasov soil type for Es = 50MPa

4.3.3. *Effect of the stiffnesses of the surrounding soil on deflections of a plate*

Figure 10 illustrates the effect of the stiffnesses of the surrounding soil on the dynamic response of a plate along axis $y = b/2$ for the modified Vlasov soil type. Between the results corresponding to the case where the stiffness of the surrounding soil is not taken into account and the case where it is taken into account, the curves appear almost mixed up both for the dynamic and static cases. Thus, the stiffness of the surrounding soil is found to have no significant effect on the deflection of the plate. This finding is inconsistent with the analysis of free vibrations, which were studied earlier [2].

4.3.4. *Effect of damping of soil*

Figures 1113 show that for different types of soil, deflection amplitudes decrease progressively as the load moves away from the observation point (x = 0, y = b/2). This is observed both when the system is considered both damp and not damp. In both cases, deflection maximizes in the vicinity of the point of application of the load. It should be noted that when a system is considered damp, the deflections are lower than those on the three types of soil (Winkler, modified Vlasov and Pasternak soils) that are not considered to be damp. This suggests that it is important to take into account the effect of damping of soil when conducting a

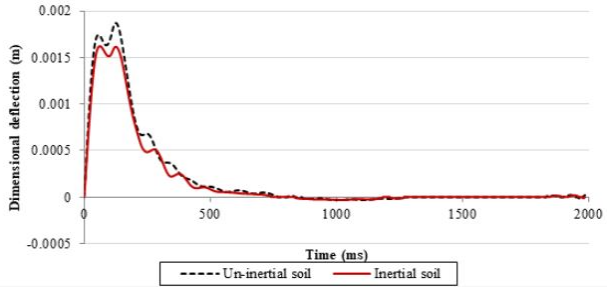

Fig. 9. Effect of inertia on a modified Vlasov soil type for Es = 75MPa

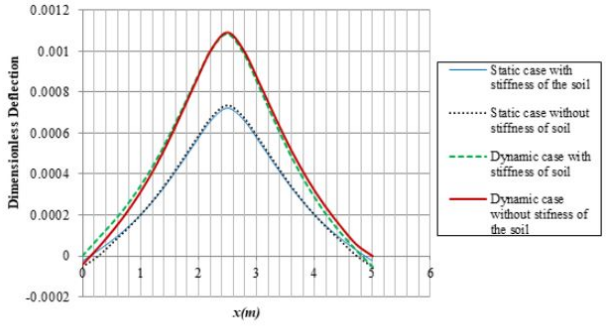

Fig. 10. Effect of plate stiffness on the deflection

dynamic analysis of a modeled plate, as shown in Figure 1.

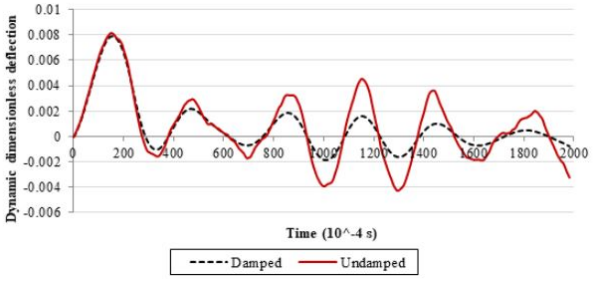

Fig. 11. Influence of damping on Winkler's soil.

5. Conclusion

This study aims to combine the DSC method and Taylor series approach with the Newmark scheme to investigate the influence of the stiffness of surrounding soil, the thickness of a plate and the depth of subsoil on the static and dynamic deflection of a thin rectangular plate. The plate is assumed to have dowelled edges and resting on a modified Vlasov soil type.

To apply the BCs and eliminating the fictitious points outside the physical domain of the plate, Taylor series ex-

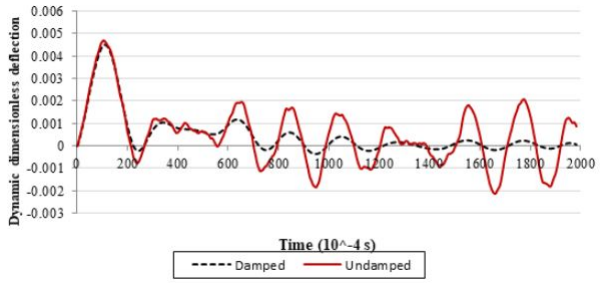

Fig. 12. Influence of damping ratio on the Pasternak soil

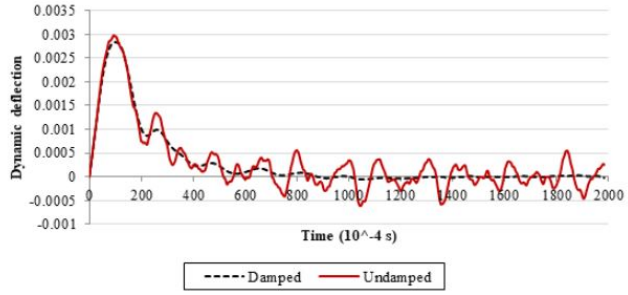

Fig. 13. Influence of damping on the modified Vlasov soil

pansion was implemented in the DSC method. By this approach, the complexity in applying the BCs at the corner points was tackled by specifying the value of torsional stiffness at the corners. The Newmark approach, on the other hand, is used to perform time integration step by step. The main conclusions of this study are listed as follows:

- With a relative error of 0.18% (with respect to Navier's method), the DSC-T in combination with the asymptotic approach could be recommended for the engineering (static) design of civil structures.
- A linear relationship can be found between the value of the logarithmic decrement of the modified Vlasov soil and soil depth.
- Beyond a certain depth, the effective soil depth, and the deflection of a plate does not vary consistently and, hence, soil can be modeled as a finite medium.
- For static loading, the deflections of a plate are more significant on the Winkler soil type with a difference of 18.83% compared to deflections on the Pasternak soil; with respect to deflections on the Vlasov soil, deflections on the Winkler soil generated a difference of 14.72%. This shows that the plate is oversized on Winkler's soil.
- Comparing the dynamic case with the static one, we deduced that the dynamic case has a significant effect on a dynamic system's response. Therefore, it is important to consider the dynamic effect of loading when designing dynamic systems.
- The effect of the inertia of soil depends on the modulus of elasticity of soil.
- For the three types of soil (Winkler, modified Vlasov and Pasternak soils), it is important to take into account the effect of damping of soil when conducting a dynamic analysis of plates.

Data Availability

The editable version of the numerical calculation code used to support the findings of this study is included in the supplementary materials file. The other numerical data used to support the findings of this study are included in the article.

Conflicts of Interest

The authors declare that they have no conflicts of interest.

Supplementary materials

The supplementary materials file contains one section that contains the Program of determination of logarithmic decrement. This section deals with the Mathematica editable code for the determination of the parameter of soil named logarithmic decrement of the soil.

Funding statement

The present research did not receive specific funding. This research work was performed as part of the employment of the authors. All the authors are working in public universities of the Republic of Benin ("University of Abomey-Calavi" and "National University of Sciences, Technologies, Engineering and Mathematics of Abomey"). Benin's public universities depend on the Ministry of Higher Education and Scientific Research.

References

[1] Ömer Civalek. Nonlinear analysis of thin rectangular plates on Winkler-Pasternak elastic foundations by DSC-HDQ methods. *Applied Mathematical Modelling*, 31(3):606–624, mar 2007.

[2] Mohamed Gibigaye, Crespin Prudence Yabi, and Gerard Degan. Free vibration analysis of dowelled rectangular isotropic thin plate on a Modified Vlasov soil type by using discrete singular convolution method. *Applied Mathematical Modelling*, 61:618–633, sep 2018.

[3] Korhan Ozgan. Dynamic analysis of thick plates including deep beams on elastic foundations using modified Vlasov model. *Shock and Vibration*, 20(1):29–41, 2013.

[4] Mohamed Gibigaye, Crespin Prudence Yabi, and I. Ezéchiel Alloba. Dynamic Response of a Rigid Pavement Plate Based on an Inertial Soil. *International Scholarly Research Notices*, 2016:1–9, 2016.

[5] S.W. Alisjahbana and W Wangsadinata. Dynamic analysis of rigid roadway pavement under moving traffic loads with variable velocity. *Interaction and multiscale mechanics*, 5(2):105–114, jun 2012.

[6] Xinwei Wang and Zhangxian Yuan. Discrete singular convolution and Taylor series expansion method for free vibration analysis of beams and rectangular plates with free boundaries. *International Journal of Mechanical Sciences*, 122:184–191, mar 2017.

[7] Kadir Mercan, Bekir Akgöz, Çiğdem Demir, and Ömer Civalek. Frequencies Values of Orthotropic Composite Circular and Annular Plates. *International Journal Of Engineering & Applied Sciences*, pages 55–55, apr 2017.

[8] Ömer Civalek. Fundamental frequency of isotropic and orthotropic rectangular plates with linearly varying thickness by discrete singular convolution method. *Applied Mathematical Modelling*, 33(10):3825–3835, oct 2009.

[9] Sofia W. Alisjahbana, Irene Alisjahabana, Shota Kiryu, and Buntara S. Gan. Semi analytical solution of a rigid pavement under a moving load on a Kerr foundation model. *Journal of Vibroengineering*, 20(5):2165–2174, 2018.

[10] Henry Khov, Wen L. Li, and Ronald F. Gibson. An accurate solution method for the static and dynamic deflections of orthotropic plates with general boundary conditions. *Composite Structures*, 90(4):474–481, oct 2009.

[11] Qin Zhu and Xinwei Wang. Free vibration analysis of thin isotropic and anisotropic rectangular plates by the discrete singular convolution algorithm. *International Journal for Numerical Methods in Engineering*, 86(6):782–800, may 2011.

[12] Y B Zhao and G W Wei. DSC analysis of rectangular plates with non-uniform boundary conditions. *Journal of Sound and Vibration*, 255(2):203–228, 2002.

[13] Xinwei Wang and Suming Xu. Free vibration analysis of beams and rectangular plates with free edges by the discrete singular convolution. *Journal of Sound and Vibration*, 329(10):1780–1792, may 2010.

[14] C. Shu, Q. Yao, and K. S. Yeo. Block-marching in time with DQ discretization: An efficient method for time-dependent problems. *Computer Methods in Applied Mechanics and Engineering*, 191(41-42):4587–4597, sep 2002.

[15] Omer Civalek and Altug Yavas. Large deflection static analysis of rectangular plates on two parameter elastic foundations. *International journal of science and technology*, 1(1):43–50, 2006.

[16] S. Zhao, G. W. Wei, and Y. Xiang. DSC analysis of free-edged beams by an iteratively matched boundary method. *Journal of Sound and Vibration*, 284(1-2):487–493, jun 2005.

[17] S. A. Eftekhari and A. A. Jafari. Vibration of an initially stressed rectangular plate due to an accelerated traveling mass. *Scientia Iranica*, 19(5):1195–1213, oct 2012.

[18] S. A. Eftekhari. A modified differential quadrature procedure for numerical solution of moving load problem. *Proceedings of the Institution of Mechanical Engineers, Part C: Journal of Mechanical Engineering Science*, 230(5):715–731, mar 2016.

[19] S. A. Eftekhari. A note on mathematical treatment of the Dirac-delta function in the differential quadrature bending and forced vibration analysis of beams and rectangular plates subjected to concentrated loads. *Applied Mathematical Modelling*, 39(20):6223–6242, oct 2014.

[20] S. A. Eftekhari and A. A. Jafari. Numerical simulation of chaotic dynamical systems by the method of differential quadrature. *Scientia Iranica*, 19(5):1299–1315, oct 2012.

[21] S. A. Eftekhari. A differential quadrature procedure with direct projection of the heaviside function for numerical solution of moving load problem. *Latin American Journal of Solids and Structures*, 13(9):1763–1781, 2016.

[22] S. Y. Yang, Y. C. Zhou, and G. W. Wei. Comparison of the discrete singular convolution algorithm and the Fourier pseudospectral method for solving partial differential equations. *Computer Physics Communications*, 143(2):113–135, feb 2002.

[23] Y. M. Xie. An assessment of time integration schemes for non-linear dynamic equations. *Journal of Sound and Vibration*, 192(1):321–331, apr 1996.

[24] C. Runge. Ueber die numerische Auflösung von Differentialgleichungen. *Mathematische Annalen*, 46(2):167–178, jun 1895.

[25] Vu-hieu Nguyen. *Comportement dynamique de structures non-linéaires soumises à des charges mobiles*. PhD thesis, 2002.

[26] Nathan M. Newmark. METHOD OF COMPUTATION FOR STRUCTURAL DYNAMICS. *Pressure Vessels Piping Design Anal*, 2:1235–1264, 1972.

[27] Adi Ben-Israel. A Newton-Raphson method for the solution of systems of equations. *Journal of Mathematical*

Analysis and Applications, 15(2):243–252, aug 1966.

[28] WT STRAUGHAN. Analysis of plate on elastic foundation. 1990.

[29] Xinwei Wang, Yongliang Wang, and Suming Xu. DSC analysis of a simply supported anisotropic rectangular plate. *Composite Structures*, 94(8):2576–2584, jul 2012.

[30] G W Wei. Discrete singular convolution for the solution of the Fokker-Planck equation. *Journal of Chemical Physics*, 110(18):8930–8942, may 1999.

[31] G W Wei, Y B Zhao, and Yang Xiang. Discrete singular convolution and its application to the analysis of plates with internal supports. Part 1: Theory and algorithm. *International Journal for Numerical Methods in Engineering*, 55(8):913–946, 2002.

[32] Guohui Duan and Xinwei Wang. Vibration analysis of stepped rectangular plates by the discrete singular convolution algorithm. *International Journal of Mechanical Sciences*, 82:100–109, may 2014.

[33] Michel Géradin and Daniel J Rixen. *Mechanical vibrations: theory and application to structural dynamics*. John Wiley & Sons, 2014.

[34] K L Nguyen, Q T Tran, L Manin, S Baguet, and M Andrianoely. Un schéma d'intégration temporelle pour la réponse transitoire de systèmes mécaniques avec butées de contact. 2017.

[35] SETRA and LCPC. Conception et dimensionnement des structures de chaussée — guide technique. *Guide technique, Dec*, 1994.

[36] NCHRP 1-37A. Guide for Mechanistic-Emperical Design of New And Rehabilitated Pavement Structure-Final Report. Technical report, 2004.

[37] Mahmoud C. Kneifati. Analysis of plates on a kerr foundation model. *Journal of Engineering Mechanics*, 111(11):1325–1342, nov 1985.

[38] Deshin Liu and Yuwei Chen. Eigenvalue analysis of thin plate with complicated shapes by a novel infinite element method. *CMES - Computer Modeling in Engineering and Sciences*, 120(2):273–292, 2019.

[39] Zhijian Qiu, Jinchi Lu, Ahmed Elgamal, Lei Su, Ning Wang, and Abdullah Almutairi. OpenSees three-dimensional computational modeling of ground structure systems and liquefaction scenarios. *CMES - Computer Modeling in Engineering and Sciences*, 120(3):629–656, 2019.

[40] Zhiqiang Ma, Lingshuang Kong, and Xianlong Jin. An explicit-implicit mixed staggered asynchronous step integration algorithm in structural dynamics. *CMES - Computer Modeling in Engineering and Sciences*, 116(1):51–67, 2018.

[41] Huaxi Lu, Zhicheng Gao, Luyao Xu, and Bitao Wu. Effects of the convex topography on railway environmental vibrations. *CMES - Computer Modeling in Engineering and Sciences*, 118(1):177–205, 2019.

[42] Der Wen Chang, Min Ru Lee, Ming Yang Hong, and Yen Chih Wang. A simplified modeling for seismic responses of rectangular foundation on piles subjected to horizontal earthquakes. *Journal of GeoEngineering*, 11(3):109–122, 2016.

[43] Der Wen Chang, Hsin Wei Lien, and Tzuyu Wang. Finite difference analysis of vertically loaded raft foundation based on the plate theory with boundary concern. *Journal of GeoEngineering*, 13(3):135–147, 2018.